Soft Matter

RSC Publishing

PAPER

View Article Online
View Journal | View Issue

Cite this: *Soft Matter*, 2013, **9**, 2518

Two-dimensional colloidal networks induced by a uni-axial external field

Heiko Schmidle,[a] Sebastian Jäger,[a] Carol K. Hall,[b] Orlin D. Velev[b] and Sabine H. L. Klapp*[a]

Received 25th September 2012
Accepted 21st December 2012

DOI: 10.1039/c2sm27210e

www.rsc.org/softmatter

Based on Monte Carlo and Molecular Dynamics computer simulations we investigate the aggregation patterns and dynamics of model colloidal mixtures consisting of particles with either one or two, oppositely oriented, induced dipole moments. The mixtures are confined to two spatial dimensions. Our model is inspired by recent optical-microscopy experiments involving polystyrene particles with (and without) gold patches. For a broad range of parameters, we find the model systems to self-assemble *via* a two-step scenario involving first percolation along the field, followed by a percolation transition in the *transverse* direction. The resulting two-dimensional networks are characterized by strongly hindered translational dynamics.

1 Introduction

Understanding the directed self-assembly of colloidal particles in external fields is at the heart of many problems in materials science, *e.g.*, the bottom-up fabrication of complex microstructures by design,[1,2] and in biology, *e.g.*, for cell sorting.[3,4] At the same time, directed self-assembly raises fundamental questions related to percolation, phase transitions, gel/glass formation, and more generally to the link between microscopic and macroscopic material properties in (field-driven) colloidal systems.[5–8] Prime examples of structures generated by directed self-assembly are one-dimensional (1D) chains,[9–13] 2D- and 3D-crystals[9,12–15] as well as sheet- and membrane-like structures[16,17] formed by polarizable (superparamagnetic) particles in electric (magnetic) fields. Microscopically, all of these structures originate from the field-induced, anisotropic dipole–dipole interactions and their interplay with the external field. The resulting structural effects have been extensively studied by theory (see *e.g.*, ref. 18–21) and simulations (see *e.g.*, ref. 10, 22 and 23).

Compared to the structures formed by "simple" particles with permanent or induced dipole moments, our theoretical understanding of (field-driven) assembly of particles with multipolar interactions is in its infancy.[24] This is in contrast to the significant experimental progress that has been made in synthesizing novel colloidal particles with tunable directional interactions. If such systems are, in addition, susceptible to an external field, new and unexpected structures can be formed. A prime example is the assembly of Janus and patchy metallodielectric particles[25] recently characterized by one of us using optical microscopy.[26] Due to induced *multipolar* (rather than dipolar) interactions which are frequency-dependent, such metallodielectric particles can form not only field-aligned chains but also chains and long clusters *perpendicular* to the field.[26] In other words, a uniaxial electric field induces here a 2D network with strongly anisotropic properties. A similar behavior (although less pronounced) has been observed in a few other systems such as mixtures of dielectric particles[27,28] and micellar systems.[17] An ultimate example of a natural system with multipolar short-range electrostatic interactions is presented by globular proteins which crystallize into different symmetries depending on the surface charge distribution.

While the synthesis and field-driven structuring of multipolar and patchy particles have been demonstrated in small 2D experimental cells, the complexity and cost of these studies pose the need for better and broader fundamental understanding of such systems, which would guide their scale-up and practical development. In the present paper we uncover by computer simulations the physical mechanism of 2D network formation by multipolar particles in uniaxial fields on the basis of a novel theoretical model. In broad correspondence with the experimental work in ref. 26, we consider a mixture of spherical particles confined to two dimensions. The particles have either one or two, oppositely oriented dipole moments. Using a combination of Monte Carlo (MC), Molecular dynamics (MD) and Langevin dynamics (LD) techniques, we demonstrate that the model indeed displays both 1D and 2D network formation, with these two structures transforming into one another by percolation transitions. Moreover, the percolated and interconnected nature of the networks leads to signatures of gel-like dynamics.

The remainder of the paper is organized as follows. In Sections 2 and 3 we present some details about our

[a]*Institute of Theoretical Physics, Technical University Berlin, Hardenbergstr. 36, 10623 Berlin, Germany. E-mail: klapp@physik.tu-berlin.de*

[b]*Department of Chemical and Biomolecular Engineering, North Carolina State University, Raleigh, North Carolina, 27695, USA*

experimental system and introduce the theoretical model on which our simulations are based. Numerical results are presented in Section 4. We close the paper in Section 5 with a brief discussion of the broader importance of the results and conclusions.

2 Experimental system

The experimental system[26] provides a basic example of multi-directional induced dipole interactions leading to the assembly of complex soft matter networks. It involves polystyrene particles with single gold patches covering 11% of their surfaces. These metallodielectric particles are dispersed in deionized water and are confined between two glass plates, yielding a quasi-2D (thin-film) geometry. The systems are exposed to an AC (alternating current) in-plane electric field, $\boldsymbol{E}$, yielding induced multipole moments in the particles and, consequently, highly anisotropic pair interactions.

Interestingly, the character of the induced multipole moments (and thus, interactions) strongly depends on the frequency (f), the physical reason being the frequency dependence of the polarizability of the two particle domains. In particular, while the gold patch is strongly polarized at any f, the polarizability of the dielectric part (together with its counterionic atmosphere) strongly depends on f and can even switch its sign. As a consequence one finds that, at $f \lesssim 200$ kHz, the external fields induce dipoles parallel to the field direction in both the polystyrene part of the particles and in the gold patch. This changes at high frequencies ($f \gtrsim 200$ kHz), where the dipoles induced in the patch and the core are similar in magnitude but *opposite* in direction.[26] The resulting "double-dipoles" within the particles yield quadrupole-like pair interactions, favoring, in particular, side-by-side configurations with the dipolar axes of the double dipoles on the two particles being parallel and the vector $\boldsymbol{r}_{ij}$ connecting the two particles being perpendicular to $\boldsymbol{E}$. This preference is in strong contrast to the typical head-to-tail ordering ($\boldsymbol{r}_{ij} \parallel \boldsymbol{E}$) of polystyrene particles without a gold patch, where only one dipole is induced. Both types of interactions, "double-dipole" and "single-dipole", are expected to be present in the experimentally investigated colloidal system, where due to imperfections in the synthesizing process, some particles are shielded during the metal deposition and it can be estimated that only 80–90 percent of the particles actually have a well-formed gold patch.

3 Theoretical model

Inspired by the real system, we investigate here a 2D binary mixture of hard spheres with equal diameters σ but different internal polarization patterns. Particles of the first species (representing the pure polystyrene) are modeled with a single, induced dipole (ID) $\boldsymbol{\mu}_i$ in their centers. The orientation of this induced dipole moment is fixed along the direction determined by the in-plane field $\boldsymbol{E}$; the magnitude of the dipole moments is assumed to be fixed as well. Particles of species 2 (representing the metallodielectric spheres) have an induced "double" dipole (DID) where the two induced dipoles are positioned side-by-side, but are antiparallel. We assign randomly if the left (right) dipole points parallel (antiparallel) to the field, thereby mimicking the fact that in the experimental system, the gold patches position themselves relative to $\boldsymbol{E}$ either on the left or right side of each patchy particle.[26] Moreover, to restrict the parameter space, the two induced dipoles in our DIDs are located symmetrically around the center, with a lateral distance of $\delta = 0.5\sigma$ between them. Both the ID and DID particles are sketched in Fig. 1 (arrows represent the induced dipole moments). The dipole moments of different particles interact *via* the usual (point) dipole–dipole potential $u_{\mathrm{DD}}(12) = {r_{12}}^{-3}[\boldsymbol{\mu}_1 \cdot \boldsymbol{\mu}_2 - 3(\boldsymbol{\mu}_1 \cdot \boldsymbol{r}_{12})(\boldsymbol{\mu}_2 \cdot \boldsymbol{r}_{12})/{r_{12}}^2]$. The resulting pair interactions between two identical DIDs and between a DID and an ID, respectively, are visualized in Fig. 1(a) and (b). For two identical DIDs, the interaction is most attractive in the side-by-side configuration, followed by a (weakly attractive) head-to-tail arrangement. The energy difference between these two configurations is, as Fig. 1(a) illustrates, about 4–$5k_{\mathrm{B}}T$ (with k_{B} and T being Boltzmann's constant and true temperature, respectively). This is close to the value of $6k_{\mathrm{B}}T$ calculated for the experimental system.[26]

To find the ground state structures of a cluster of a few ($N = 3$–5) such particles, we used simulated annealing (SA) involving several independent runs per system (for related ground state calculations involving systems with "simple" dipoles, see ref. 29 and 30). The SA method is based on a standard Metropolis scheme where, however, T is lowered to zero step by step. The resulting configurations are shown in the bottom row of Fig. 1. For three equally oriented DIDs, the lowest-energy configuration is still a chain oriented perpendicular to $\boldsymbol{E}$, whereas $N \geq 4$ DIDs form compact clusters with square-like local structures [see Fig. 1(c) and (d)]. For two *oppositely* oriented DIDs the interaction energy is just the inverse of the one shown in Fig. 1(a), yielding a preference for "staggered" configurations

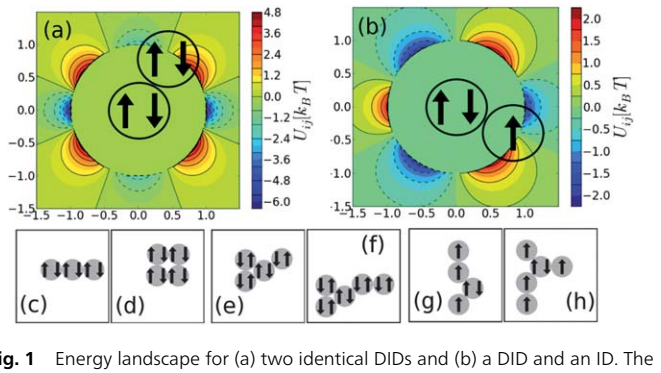

Fig. 1 Energy landscape for (a) two identical DIDs and (b) a DID and an ID. The numbers on the horizontal and vertical axes give the distance between the two particles in x- and y-directions in units of σ. In both part (a) and (b), a DID is sitting at the center. The solid circle indicates its diameter of 1σ. The second particle is drawn at an off-center position in the right upper segment (a) or right lower segment (b), respectively. The "empty" ring around the DID in the center indicates that the second particle cannot come closer than 1σ. The color code gives the value of the interaction energy of the two particles depending on their configuration in units of $k_{\mathrm{B}}T$ [see bars at the right side of (a) and (b)]. (c–h) Ground state structures involving identical DIDs (c and d), oppositely oriented DIDs (e and f), and DID–ID mixtures (g and h).

where $\boldsymbol{r}_{ij}$ makes an angle of $\theta_{ij} = 35^{\circ}$ with the field. The resulting cluster configurations are shown in Fig. 1(e) and (f). Finally, the interactions between a DID and an ID lead to a "triangular" arrangement as illustrated in Fig. 1(b). That is, an ID next to a central DID favors either a side-by-side configuration or a shifted configuration with $\theta_{ij} = 50^{\circ}$. As revealed from Fig. 1(g) and (h), in mixed DID–ID systems the IDs form vertical chains with laterally shifted DIDs between them. We note, in particular, that four IDs plus one DID form a "Y-like" connection [see Fig. 1(h)]. Interestingly, triangular cluster structures such as the one shown in Fig. 1(e) have also been found in other non-standard dipolar models, such as 2D systems of spheres with off-centered (permanent) dipole moments.[31]

Another interesting question is to what extent the DID ground-state configurations shown in Fig. 1(c)–(h) also reflect the energetically favorable configurations of particles with *point quadrupoles*. In other words, how important (for the modeling of the real system) is the fact that the two dipoles characterizing our DIDs are spatially separated? Indeed, an analysis of some relevant pair configurations of point quadrupoles reveals that such particles prefer side-by-side configurations, as do two DIDs [see Fig. 1(a)]. However, an important difference between the models is that the DID attraction in the side-by-side configuration is three times larger than in the head-to-tail configuration, while for point quadrupoles, these two configurations have similar attraction strength. We thus expect that our model has a stronger tendency to form "cross links" between field-aligned chains than a purely quadrupolar model. Moreover, the DIDs appear to be somewhat more realistic (than using a point quadrupole) due to the two-component, "patched" character of the real particles.

To explore the system's behavior at finite temperatures $T^* = k_B T\sigma^3/\mu^2$ we performed canonical MC simulations with up to 900 particles. The simulations are carried out using periodic boundary conditions in both spatial directions. The long-range dipolar interactions are taken into account *via* the two-dimensional Ewald summation technique. Further simulation details can be found in ref. 23.

4 Results and discussion

4.1 Structure formation

The mixtures of DIDs and IDs are characterized by the total density $\rho = \rho_{DID} + \rho_{ID}$ and concentration of DIDs $c_{DID} = \rho_{DID}/\rho$. Regarding the total density, we typically use the dimensionless quantity $\rho^* = \rho\sigma^2$. Two typical MC simulation "snapshots" at a temperature corresponding to strong electrostatic coupling ($T^* = 0.15$) and two parameter sets (ρ^*, c_{DID}) are shown in Fig. 2 along with two images of the experimental system.

Both experimental images (left panels) have been obtained at an AC frequency of $f = 400$ kHz (*i.e.*, above the threshold for induced DIDs); they differ by the field strength and the surface packing fraction $\phi = (\pi/4)\rho^*$. The latter are $\phi \approx 0.23$ ($\rho^* = 0.29$) and $\phi \approx 0.38$ ($\rho^* = 0.48$) as shown in Fig. 2(a) and (b), respectively, which is comparable to the values considered in our simulations. At low packing fractions, most particles in the experiment [see Fig. 2(a)] are arranged into long chains in the field direction. These chains are partially linked by "T-like" connections (perpendicular to $\boldsymbol{E}$) and staggered-chain ("Y-like") configurations. The system is percolated along the field, whereas no connecting path (and thus, no percolation) appears in the transverse direction (*i.e.*, perpendicular to $\boldsymbol{E}$). A similar scenario is seen in our model system for $\rho^* = 0.25$ and $c_{DID} = 0.25$, as illustrated in Fig. 2(c). Here, the vertical chains consist predominantly of IDs whereas the T- and Y-connections originate from DID–DID and DID–ID interactions, respectively, which is consistent with the ground state configurations depicted in Fig. 1. At higher packing fractions the amount of T- and Y-connections in the experimental system increases [see Fig. 2(b)] to the extent that the structures become percolated in a *two-dimensional*, anisotropic network of cross-linked chains. The same happens in the MC simulations, if we increase (along with an increase of ρ^*), the DID concentration to $c_{DID} = 0.5$. A closer inspection of the experimental snapshot reveals that the ratio of T- to Y-connections is significantly larger than in the simulations, leading to an overall more rigid structure. We assume that this is a consequence of the fact that both c_{DID} and the coupling strength $1/T^*$ are larger in the real system; however, mimicking this situation in the simulations requires (as we have tested explicitly) much longer computational times while not providing significant additional insights. Nevertheless, the results of the simulation are in excellent visual agreement with the experimental data involving real patchy microspheres.

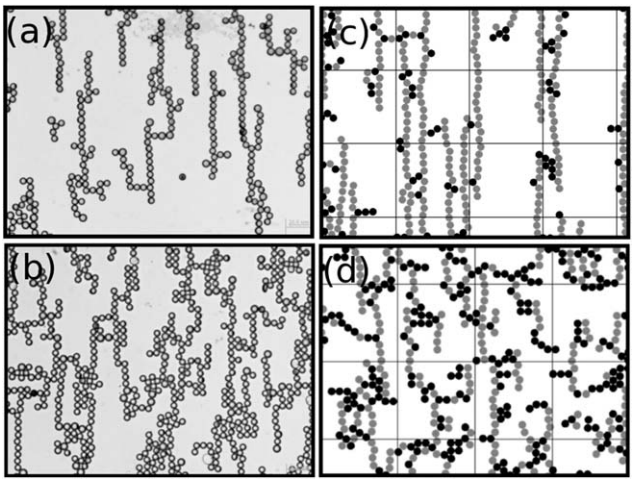

Fig. 2 (a and b) Optical microscopy images of the experimental system of 5 μm particles similar to the one studied in ref. 26 at a frequency $f = 400$ kHz and two sets of field strengths and total densities [(a) $\rho^* = 0.29$, (b) $\rho^* = 0.48$]. Right: MC simulation "snapshots" of model mixtures at $T^* = 0.15$ and (c) $c_{DID} = 0.25$, $\rho^* = 0.25$, (d) $c_{DID} = 0.5$, $\rho^* = 0.4$. In parts (c) and (d), the IDs and DIDs are represented as grey and black spheres, respectively.

4.2 Percolation

Given the two types of percolated structures observed in theory and experiment, we now explore whether these structures are separated by a *percolation transition*. The relevant order parameters in this context are the probabilities $\Pi_{\parallel}$ and $\Pi_{\perp}$ of

finding a cluster that reaches from one side of the box to the opposite side, along or perpendicular to the field. We consider two particles to be associated into the same cluster if the distance between the spheres is smaller that the critical radius, R_c.[15] This critical radius is set to $R_c = 1.25\sigma$ (for a similar choice, see ref. 32). Test calculations indicate that the results for the percolation probabilities are not very sensitive to the specific value of R_c.

In the following we consider two systems at the same concentration ($c_{DID} = 0.25$) but different densities $\rho^* = 0.25$, $\rho^* = 0.5$. The corresponding MC data for $\Pi_{\parallel/\perp}$ as functions of T^* are plotted in Fig. 3. To control finite-size effects, all calculations have been done with three values of N. For both $\rho^* = 0.25$ and $\rho^* = 0.5$, the steep increase of $\Pi_\parallel$ towards values close to one upon lowering T^* [see Fig. 3(a)] clearly reveals the existence of a longitudinal percolation transition along the field. As expected, the transition temperature (estimated from the intersection of the curves related to different N) is somewhat higher at $\rho^* = 0.5$. Only the latter system displays additionally a transverse percolation transition where the 1D percolated structure transforms into a 2D network. This is seen from the curve $\Pi_\perp(T^*)$ in Fig. 3(b); the corresponding values of $\Pi_\perp$ at $\rho^* = 0.25$ are negligible. We note that the transverse percolation can also be found at lower total densities if we increase c_{DID} accordingly (thereby favoring crosslinking). The interplay between total density and concentration is illustrated in Fig. 4 where we show, for various values of the concentration of DIDs (c_{DID}) $\Pi_\parallel$ and $\Pi_\perp$ as functions of the total density. The reduced temperature is fixed to $T^* = 0.15$ (corresponding to a value where the systems considered in Fig. 3 are deep within the percolated regime). From Fig. 4, it is seen that percolation in the transverse direction occurs already for a very small DID concentration ($c_{DID} = 0.1$), with the corresponding percolation threshold being, however, rather high ($\rho^* \approx 0.45$). For the same system, the percolation *longitudinal* to the field occurs already at $\rho^* = 0.1$. Upon increasing the DID concentration, the two thresholds approach one another (see data for $c_{DID} = 0.25$ and $c_{DID} = 0.5$). In other words, an increase of the fraction of simple dipolar particles raises the concentration threshold needed for transverse percolation in the system. However, once this threshold is reached the system will be more prone to forming a mechanically stronger, bi-directional crosslinked gel.

The structural changes before and after the two percolation transitions are visible from Fig. 5(a) and (b) where we plot the pair correlation functions parallel and perpendicular to $\boldsymbol{E}$, $g_{\parallel/\perp}(r)$, at $\rho^* = 0.50$, $c_{DID} = 0.25$, and three temperatures. Regarding $g_\parallel$, a comparison of the curves at $T^* = 0.5$ and 0.3 shows that the longitudinal percolation transition leads to strong peaks at multiples of σ. Below the transverse percolation transition ($T^* = 0.15$) one observes additional small peaks in between the main peaks. These peaks reflect the presence of "triangular" connections, in which one DID is arranged to the right or left of two IDs forming (parts of) a chain [*cf.* Fig. 1(g) and (h)]. Interestingly, the function $g_\perp$ behaves different from $g_\parallel$ in the sense that its structure rather weakens upon lowering T^*. This may be explained as follows: at temperature $T^* = 0.5$ the DIDs build larger clusters than the IDs due to their stronger mutual coupling. Decreasing T^*, the IDs start to form rigid chains, thereby hindering the self-assembly of the DIDs into compact clusters. Rather, the DIDs form short connections between the ID chains (see snapshot in Fig. 2), which results in a less pronounced $g_\perp(r)$ below the second transition.

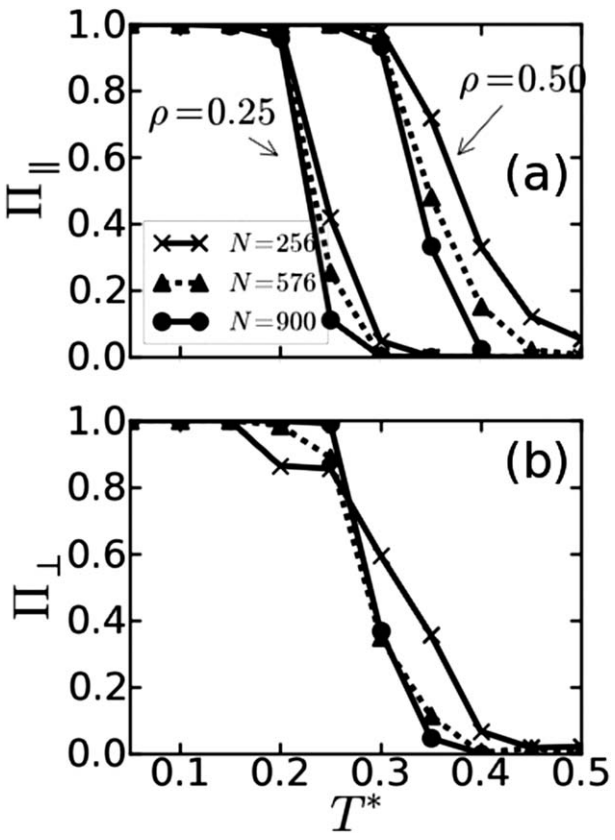

Fig. 3 (a) Percolation probability parallel to $\boldsymbol{E}$ as a function of T^* at $\rho^* = 0.25$, 0.5 and different system sizes ($c_{DID} = 0.25$). (b) Percolation probability perpendicular to $\boldsymbol{E}$ at $\rho^* = 0.5$.

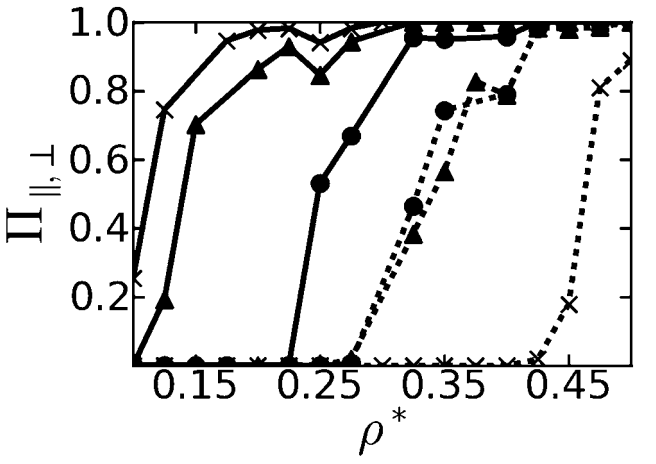

Fig. 4 Percolation probability in the field direction (solid lines) and perpendicular to it (dashed lines) as a function of the total density. The fraction of DID in the system is $c_{DID} = 0.5$ (circles), 0.25 (triangles) and 0.1 (crosses).

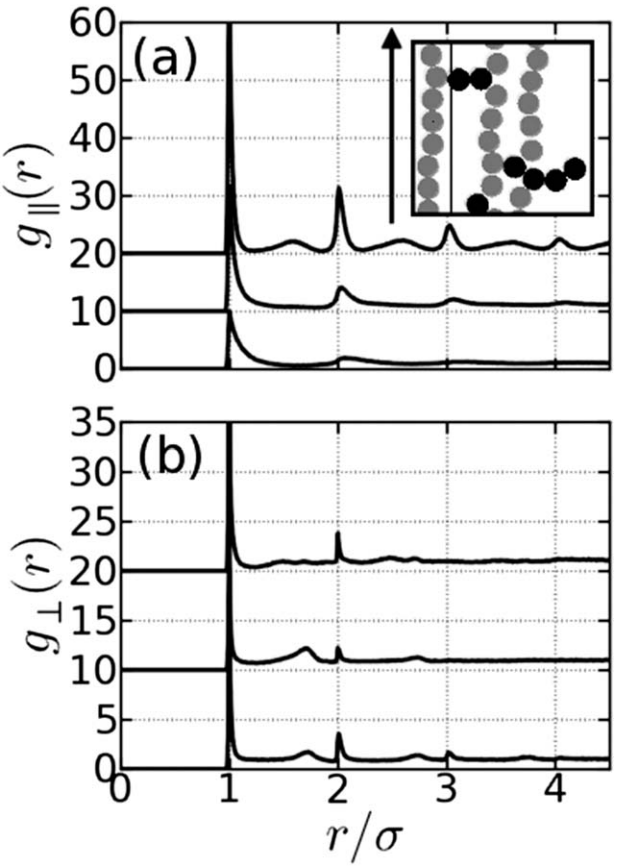

Fig. 5 Parallel (a) and perpendicular (b) pair correlation function at $T^* = 0.15$, 0.3 and 0.5 (from top to bottom, curves are shifted to enhance visibility). The total density and concentration are $\rho^* = 0.5$ and $c_{DID} = 0.25$, respectively. The inset in (a) corresponds to the structure also shown in Fig. 2(c). The arrow indicates the direction of the external field.

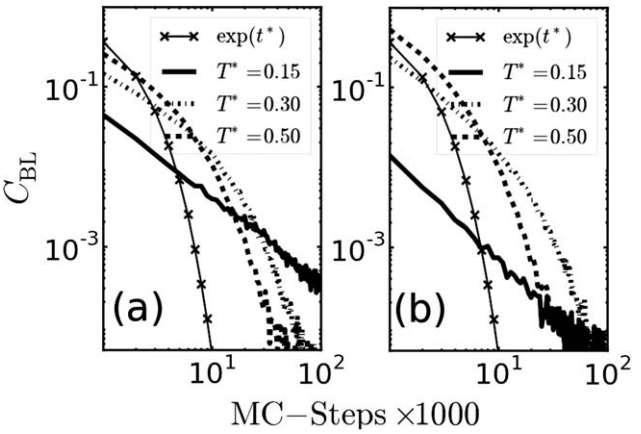

Fig. 6 Bond correlation function as a function of dimensionless time t^* at (a) $\rho^* = 0.25$ and (b) $\rho^* = 0.5$ (and different T^*) along with an exponential function ($c_{DID} = 0.25$).

4.3 Persistence of the network and translational dynamics

Given the cross-linked network formed at temperatures below the transverse percolation threshold, it is interesting to investigate the persistence of this network. The persistence will be particularly important for the mechanical properties of the network. To characterize the persistence we calculate the bond correlation function $c_{BL}(t)$ measuring the lifetime of bonds between two particles. We obtain this time-dependent function by MC simulations, making use of a recently established connection[32] between MC and (overdamped) Brownian Dynamics simulations.[16] To evaluate $c_{BL}(t)$, we assign a variable $n_{ij}(t)$ to each pair of particles, which is 1 if the particles i and j are bonded[15] and zero if not. The bond correlation function is then defined as $c_{BL}(t) = \langle n_{ij}(t) n_{ij}(0) \rangle$, averaged over all pairs ij. In Fig. 6 we present data for $c_{BL}(t)$ [where time is measured in MC steps] at $\rho^* = 0.25$ and 0.5. The concentration of DIDs is set to $c_{DID} = 0.25$.

At temperatures above the longitudinal percolation ($T^* = 0.5$), c_{BL} decays essentially exponentially. A similar behavior is found at $T^* = 0.3$ which is below the longitudinal percolation threshold at $\rho^* = 0.5$ (but above this threshold at $\rho^* = 0.25$). At the low temperature $T^* = 0.15$, however, we find at both densities dramatically different behaviors indicative of gelation. Specifically we discover the power-law decay, that is, $c_{BL} \sim (t^*)^{-\alpha}$, with $\alpha = 1.09 \pm 0.04$ (1.36 ± 0.04) at $\rho^* = 0.25$ (0.5). This power-law behavior is somewhat different than that of gel-forming 3D dipolar systems, where $c_{BL}(t)$ displays a stretched exponential behavior.[6,7,33] We cannot exclude that this difference is just due to insufficient long-time statistics of our data. Irrespective of the exponent, however, our data show that the bond lifetime in the crosslinked network is extremely long, suggesting a strong persistence of the network. Moreover, it is interesting to observe that at $T^* = 0.15$, where both systems are percolated in perpendicular directions, the bond correlation function relaxes to zero faster at the larger density; in other words, the low-density system is characterized by a longer relaxation time. This resembles the behavior reported in a recent simulation study of the three-dimensional dipolar hard sphere model.[33]

A further interesting aspect concerns the translational dynamics of the particles. The translational mobility is important for transport properties such as conductivity of the material. As shown in Section 4.2, the present model displays one main ingredient of gelation, that is, percolation.[8] Therefore, one may expect signatures of gel-like dynamics in quantities such as the intermediate scattering function and the translational mean-squared displacement, similar to what has been observed in other dipolar, network-forming systems.[5,6] Here we focus on the mean-squared displacement (MSD).

To calculate this quantity we have performed MD simulations, using the same dipolar/quadrupolar potential as in the MC simulations but with the hard-core being replaced by a steep continuous repulsion $\propto (\sigma/r)^{28}$. Our motivation to use MD rather than MC to calculate the MSD was that we did not want to restrict ourselves to the case of overdamped Brownian motion, which is implicitly assumed when using MC.[32]

We have calculated the MSD parallel and perpendicular to the field, $\Delta \boldsymbol{r}_{\gamma}{}^2(t) = N^{-1} \sum_i \left\langle (\boldsymbol{r}_{i,\gamma}(t) - \boldsymbol{r}_{i,\gamma}(0))^2 \right\rangle$ as a function of time t, with $\gamma = \parallel$ or $\gamma = \perp$. MD results for the density $\rho^* = 0.5$ and three temperatures are plotted in Fig. 7(a) and (b).

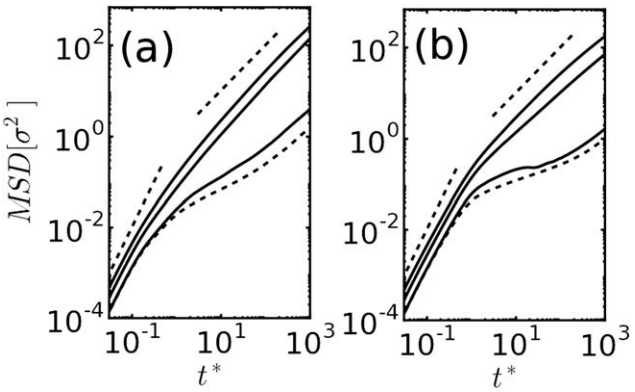

Fig. 7 MSD parallel (a) and perpendicular (b) to the field as a function of dimensionless time t^* at $\rho^* = 0.5$, $c_{DID} = 0.25$, and $T^* = 0.5$, 0.3, 0.15 (from top to bottom). The dashed straight lines indicate pure ballistic (small t^*) and diffusive behavior (large t^*). The lowermost dashed line corresponds to Langevin Dynamics results ($T^* = 0.15$).

At short times all curves exhibit the expected ballistic behavior ($\propto t^2$), whereas the dynamics at intermediate times is strongly temperature-dependent. Specifically, for $T^* = 0.5$, *i.e.*, above the longitudinal percolation transition, and for $T^* = 0.3$ (between the longitudinal and transverse transition), the MSDs reveal a normal diffusive behavior $\propto t$, with the extracted long-time diffusion constants being somewhat larger along than perpendicular to the field, that is, $D_{\parallel} > D_{\perp}$. Below the transverse percolation transition ($T^* = 0.15$), however, the dynamics dramatically changes: here the MSDs, and particularly the one in the perpendicular direction, exhibit a pronounced plateau. These plateaus reflect that the cross-linking of vertical chains due to the DID particles [which is also seen in the pair correlations, see Fig. 5(a)] leads to a strongly hindered translational diffusion. The length scale related to the plateau in the transverse MSD is in the range of $\sim 0.1\sigma$ known from colloidal gels in three dimensions.[5,6] Only at very long times, the MSD tends towards the linear time dependence expected for "normal" diffusion. To estimate the extent to which a fluid medium (*i.e.*, a solvent) would influence these results we performed Langevin dynamics simulations, with different input friction coefficients. Even for the strongest friction considered (where the corresponding diffusion constant is in the range suggested by the MD data), the MSDs are characterized by plateaus [see Fig. 7]. This suggests that the hindered dynamics persists even in the presence of a medium.

5 General discussion and conclusions

To our knowledge this is the first realistic simulation of the network formation in systems where mixtures of patchy and regular particles are subjected to an external field. Our simulations demonstrate that "patchy" particles with multipolar interactions mixed with simple dipolar particles can form percolated, gel-like structures both parallel and perpendicular to the field, which is consistent with recent experiments on metallodielectric particles.[26] The transformation between these structures takes place *via* two clear, longitudinal and transverse percolation transitions, with the novel 2D-crosslinked structure being stable for a broad range of concentrations and coupling strengths. The longitudinal chaining is a common property of magnetorheological and electrorheological fluids, while the transverse crosslinking and percolation observed experimentally and fundamentally characterized here are new features brought forward by the patchy particles with multipolar interactions. These features have the potential to drastically increase the elastic response and lead to the formation of strongly gelled systems at low particle volume fractions. The simulations reveal how the degree of crosslinking and gelation can be made tunable by the composition, where the patchy particles are the key to the transversal crosslinking of chains. This could allow the formulation of a means of control of the viscosity, gelation and solidification thresholds of particle suspensions in external fields.

Our simulation results may be taken as a guideline for future, systematic experiments and the design of tailored microstructures, at concentrations and ratios of the dipolar and patchy particles that can now be optimized with regard to the desired structural and gelation transitions. Given the strong and composition-dependent anisotropy of our networks (with respect to $\boldsymbol{E}$) the models could also allow progress towards field-directed synthesis of materials with anisotropic porosity, tunable thermal and electrical conductivity and other uncommon mass-, heat-transport and structural properties.[34,35] Finally, since mixtures of multipolar and dipolar particles can exist even in the absence of external fields, the present findings have relevance not only in the context of field-induced structuring, but also for other hybrid materials such as colloids in nematic liquid crystals.[36,37]

Acknowledgements

We gratefully acknowledge financial support from the Deutsche Forschungsgemeinschaft through the International Research Training Group 1524 "Self-Assembled Soft Matter Nano-Structures at Interfaces" (project C 3.1) and by the US-NSFs Programmable Soft Matter MRSEC (DMR-1121107). The experimental paper, ref. 26, has been possible by the contributions of Sumit Gangwal, Amar Pawar and Ilona Kretzchmar. We also thank Carlos Alvarez for helpful discussions regarding the energy landscape.

References

1 Z. Nie, A. Petukhova and E. Kumacheva, *Nat. Nanotechnol.*, 2010, **5**, 15.
2 O. D. Velev and S. Gupta, *Adv. Mater.*, 2009, **21**, 1897.
3 J. F. Douglas, J. Dudowicz and K. F. Freed, *Phys. Rev. Lett.*, 2009, **103**, 135701.
4 M. Sancho, G. Martínez, S. Muñoz, J. L. Sebastián and R. Pethig, *Biomicrofluidics*, 2010, **4**, 022802.
5 M. A. Miller, R. Blaak, C. N. Lumb and J. P. Hansen, *J. Chem. Phys.*, 2009, **130**, 114507.
6 P. Ilg and E. Del Gado, *Soft Matter*, 2010, **7**, 163.
7 E. Del Gado and W. Kob, *Soft Matter*, 2010, **6**, 1547.
8 E. Zaccarelli, *J. Phys.: Condens. Matter*, 2007, **19**, 323101.

9 O. D. Velev and K. H. Batt, *Soft Matter*, 2006, **2**, 738.
10 J. Jordanovic, S. Jäger and S. H. L. Klapp, *Phys. Rev. Lett.*, 2011, **106**, 038301.
11 A. Hynninen and M. Dijkstra, *Phys. Rev. Lett.*, 2005, **94**, 138303.
12 D. Heinrich, A. R. Goñi, A. Smessaert, S. H. L. Klapp, L. M. C. Cerioni, T. M. Osán, D. J. Pusiol and C. Thomsen, *Phys. Rev. Lett.*, 2011, **106**, 208301.
13 S. O. Lumsdon, E. W. Kaler and O. D. Velev, *Langmuir*, 2004, **20**, 2108.
14 A. Yethiraj, A. Wouterse, B. Groh and A. van Blaaderen, *Phys. Rev. Lett.*, 2004, **92**, 058301.
15 H. Schmidle, C. K. Hall, O. D. Velev and S. H. L. Klapp, *Soft Matter*, 2012, **8**, 1521.
16 S. Jäger and S. H. L. Klapp, *Soft Matter*, 2011, **7**, 6606.
17 A. B. Pawar and I. Kretzschmar, *Langmuir*, 2008, **24**, 355.
18 E. Pyanzina, S. Kantorovich, J. J. Cerda and C. Holm, *J. Magn. Magn. Mater.*, 2011, **323**, 1263.
19 V. S. Mendelev and A. O. Ivanov, *Phys. Rev. E: Stat., Nonlinear, Soft Matter Phys.*, 2004, **70**, 051502.
20 S. Klapp and F. Forstmann, *Phys. Rev. E: Stat. Phys., Plasmas, Fluids, Relat. Interdiscip. Top.*, 1999, **60**, 3183.
21 L. Luo, S. H. L. Klapp and X. Chen, *J. Chem. Phys.*, 2011, **135**, 134701.
22 J. P. Huang, Z. W. Wang and C. Holm, *Phys. Rev. E: Stat., Nonlinear, Soft Matter Phys.*, 2005, **71**, 061203.
23 H. Schmidle and S. H. L. Klapp, *J. Chem. Phys.*, 2011, **134**, 114903.
24 K. Van Workum and J. F. Douglas, *Phys. Rev. E: Stat., Nonlinear, Soft Matter Phys.*, 2006, **73**, 031502.
25 S. Gangwal, O. J. Cayre and O. D. Velev, *Langmuir*, 2008, **24**, 13312.
26 S. Gangwal, A. Pawar, I. Kretzschmar and O. D. Velev, *Soft Matter*, 2010, **6**, 1413.
27 J. L. Griffin and C. D. Ferris, *Nature*, 1970, **226**, 152.
28 V. Giner, M. Sancho, R. S. Lee, G. Martinez and R. Pethig, *J. Phys. D: Appl. Phys.*, 1999, **32**, 1182.
29 P. Jund, S. G. Kim, D. Tomanek and J. Hetherington, *Phys. Rev. Lett.*, 1995, **74**, 3049.
30 T. A. Prokopieva, V. A. Danilov, S. S. Kantorovich and C. Holm, *Phys. Rev. E: Stat., Nonlinear, Soft Matter Phys.*, 2009, **80**, 031404.
31 S. Kantorovich, R. Weeber, J. J. Cerda and C. Holm, *Soft Matter*, 2011, **7**, 5217.
32 E. Sanz and D. Marenduzzo, *J. Chem. Phys.*, 2010, **132**, 194102.
33 L. Rovigatti, J. Russo and F. Sciortino, *Soft Matter*, 2012, **8**, 6310.
34 J. Philip, P. D. Shima and B. Raj, *Appl. Phys. Lett.*, 2007, **91**, 203108.
35 G. Sun and K. Lu, *Phys. Rev. E: Stat., Nonlinear, Soft Matter Phys.*, 2011, **83**, 041405.
36 I. Muševič, M. Škarabot, U. Tkalec, S. Ravnik, M. Ravnik and S. Žumer, *Science*, 2006, **313**, 954.
37 U. Ognysta, A. Nych, V. Nazarenko, M. Skarabot and I. Muševič, *Langmuir*, 2009, **25**, 12092.

